A Feedback Model of Cyclotron Interaction between Whistler-Mode Waves and Energetic Electrons in the Magnetosphere

R. A. HELLIWELL AND T. L. CRYSTAL

Radioscience Laboratory, Stanford University, Stanford, California 94305

Cyclotron resonance is employed in a new model of the generation of narrow-band VLF emissions from the magnetosphere. Streaming energetic resonant electrons are temporarily phase-bunched by whistler-mode waves, causing transverse currents to be impressed on the medium. These currents act like circularly polarized antennas, producing stimulated Doppler-shifted radiation. The interaction takes place in an 'emission cell' located at or near the equatorial plane. Inclusion of feedback between the stimulated radiation and the incoming particles leads to a self-consistent description of fields and currents in time and space. Sample calculations are made for a wave frequency of 16.5 kHz and a homogeneous interaction region of 750-km length located on the equator at $L = 3$. When there is a 1-mγ input wave and a stream density of 2.4 m^{-3}, regular pulsations with a period of 110 msec are produced. Above a threshold stream density of 1.5 m^{-3}, self-sustained oscillations grow exponentially when the system is triggered by a short pulse. Following saturation, a steady state is reached in which the frequency bandwidth is zero. Predictions of the model are in good agreement with experimental observations.

For years, workers in magnetospheric physics have been puzzled by narrow-band VLF emissions [*Helliwell*, 1965]. Believed to originate near the equatorial plane of the magnetosphere, these signals can be triggered by whistlers, man-made signals, or other emissions. They may also occur spontaneously, often appearing in bands whose frequency is related to the electron gyrofrequency at the equator [*Burtis and Helliwell*, 1969]. When the time separation between individual emissions is small, the ensemble is called 'chorus.' A related phenomenon is the pulsation of whistler-mode signals from ground VLF transmitters [*Bell and Helliwell*, 1971; *Likhter et al.*, 1971].

Theories of VLF emissions have been based on both Cerenkov and cyclotron resonance between the waves and the energetic electrons [*Kimura*, 1967; *Gendrin*, 1972]. In the present paper we present a new theory of narrow-band VLF emissions, based on cyclotron resonance. Resonant electrons are phase-bunched by the waves so that their Doppler-shifted cyclotron radiation is coherent for a short time interval. The interaction takes place in a limited volume of space near the equatorial plane, as is shown in the sketch of Figure 1. This region will be called the 'emission cell,' or the 'interaction region.' The resonant electrons may traverse this cell several times as a result of mirroring. They are in a sense recycled until the east-west drift or diffusion into the loss cone removes them from the cell.

A novel feature of our treatment is the inclusion of feedback between waves and electrons. To simplify the computations, the continuous flow of electrons is represented by discrete current sheets, as is shown in the upper part of Figure 1. The stimulated radiation from these sheets modifies the total field, which in turn phase-bunches new electrons entering the cell. A feedback loop is thus established between the stimulated radiation and the incoming resonant electrons.

The role of phase bunching and feedback in the generation of discrete VLF emissions was first suggested by *Brice* [1963], who likened the stimulated emission to radiation from an end-fire array of circularly polarized antennas. Based on Brice's suggestion, a phenomenological theory of discrete VLF emissions was outlined [*Helliwell*, 1967], in which the spectrum of the waves and the length of the cell were estimated. In a later paper [*Helliwell*, 1970] this work was extended to include a general electron density model and variable frequency waves. In the

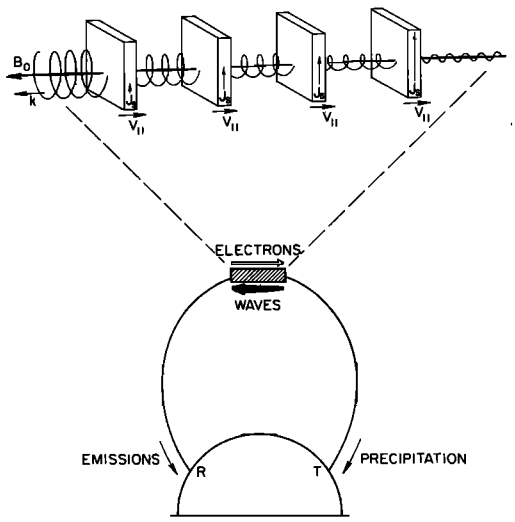

Fig. 1. Sketch of interaction region, or emission cell, model. Circularly polarized waves transmitted from T resonate with oppositely traveling electrons near the equator. The train of electron sheets represents a continuous stream of resonant electrons. The resonant electrons in each sheet are phase-bunched by the wave, producing a transverse stimulated current J_s. The change in wave amplitude shown across each sheet results from the addition of the wave component generated by J_s. Emissions travel to R, whereas scattered electrons are precipitated at T.

present paper a self-consistent description of the fields and the transverse convection currents created by these fields is obtained in space and time.

Among the results predicted by our theory are (1) amplitude pulsations for continuous wave excitation, (2) self-sustaining oscillations for stream densities above a certain 'threshold' value, and (3) a limiting amplitude for driven and self-excited oscillations. Observational data supporting these new results are cited. A suggestion is made regarding the onset of artificially stimulated emissions (ASE).

PHYSICAL MODEL

Because of the complexity of the actual physical problem, it is essential to simplify the model as much as possible. Accordingly, we have assumed a homogeneous region whose length is based on *Helliwell* [1970]. Outside this region it is assumed that the interaction can be neglected or treated independently.

The frequency of the applied wave is constant, and the envelope of its amplitude is a square-topped pulse. The pulse length can be varied from zero to infinity. The wave is assumed plane, and the direction of propagation is taken parallel to the earth's magnetic field (Figure 2). The change in field intensity of the total wave is assumed to be small in the space of 1 wavelength. The frequency of the applied wave is one-half the local electron gyrofrequency, a value typical of observed triggered emissions [*Carpenter,* 1968; *Helliwell,* 1969]. The phase and group velocities are then the same, and the streaming velocity of the electrons has the same magnitude as the phase velocity.

The interacting electrons are represented by a monoenergetic stream of resonant electrons having an initial pitch angle α of 30°. The initial values of the phase angle θ of the individual electrons of the stream are assumed to be randomly distributed, so that the net initial transverse current of the stream is negligible. To represent this random phase angle distribution, we employ 12 elementary streams of electrons (represented by their perpendicular velocity vectors shown in Figure 3*a*) spaced 30° apart in phase. Each elementary stream is assumed to extend to infinity in the transverse (x-y) plane. The orbit of each individual electron in the stream is a helix. In our model the

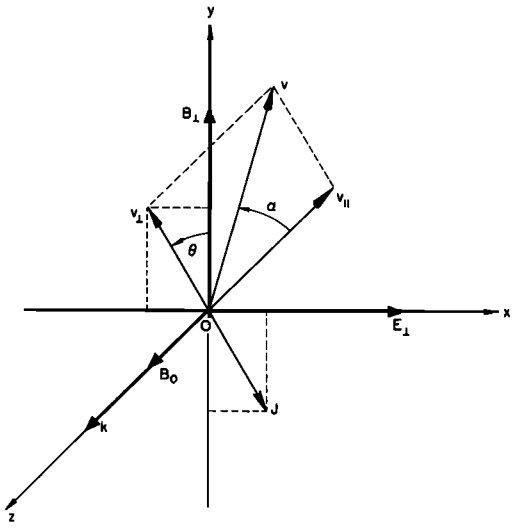

Fig. 2. Coordinate system and relation of wave fields and electron velocities.

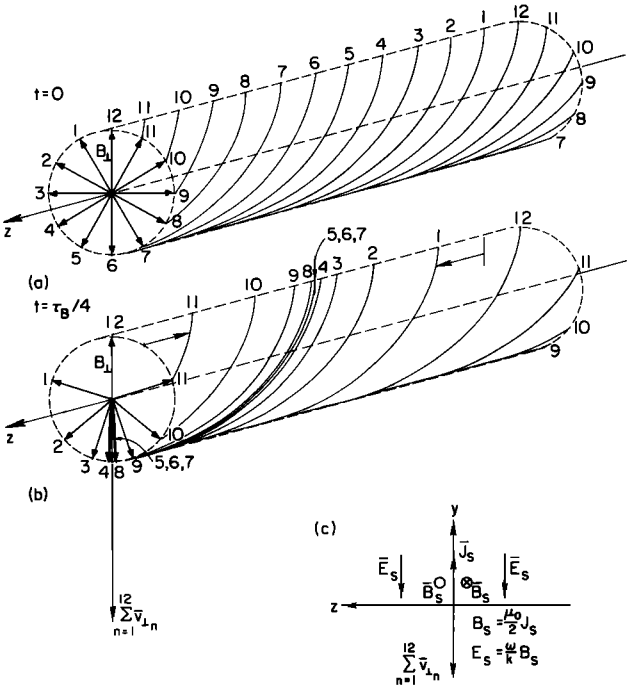

Fig. 3. Helical loci of the perpendicular velocities of 12 elementary streams (a) before bunching, (b) after some bunching ($B_\perp$ is represented by vector 12), and (c) for ensemble sheet current J_s and associated induced magnetic (B_s) and electric (E_s) fields.

orbit diameter is 153 meters and is small compared with the wavelength of 1667 meters. The perpendicular velocities in the elementary stream have approximately constant magnitude and rotate at the electron gyrofrequency. To simplify the drawing in Figure 3, both $\mathbf{B}_\perp$ and stream 12 $\mathbf{V}_\perp$ are represented by the same vector. Initially, before any bunching has occurred, the 12 helices are equally spaced (Figure 3a). At this time there is no transverse current because the vector sum of the 12 helical currents is zero.

The helical motion of the electrons constitutes a helical current that radiates a Doppler-shifted wave in the $+z$ direction. The radiation from each elementary stream is the property of the stream alone and to first order is unaffected by the wave. The main function of the wave is to organize the relative phases of the elementary streams so that their radiation becomes coherent. We neglect the wave-induced perturbations of α and $v_\perp$ because only a very small fraction of the kinetic energy of each electron can be exchanged with the wave during interaction. (We note, however, that precipitation of electrons near the loss cone into the ionosphere may be caused by just these perturbations.) For example, consider a representative resonant electron with an initial energy of 2.9 kev, an α of 30°, and a $v_\perp$ of 1.6×10^7 m/sec that is exposed to a wave electric field of 3×10^{-5} v/m. Assume that the electric field acts in a direction either parallel or antiparallel to $\mathbf{v}_\perp$ for a time of 30 msec. Then the magnitude of the change in kinetic energy of the electron is $(3 \times 10^{-5} \times 1.6 \times 10^7 \times 30 \times 10^{-3}) = 14$ volts. Accordingly, an electron either gains or loses no more than 5×10^{-3} of the available energy. From *Brice*'s [1964a] equations the corresponding change in α is 2.4°, which would modify the pitch angle distribution significantly. However, the corresponding change in $v_\perp$ is only 2%. This change is too small to have an important effect on the phase-bunched current calculation.

As the 12 streams move into the wave, they feel the bunching force $-qv_\perp B_\perp \sin \theta$, which causes each helix to move longitudinally with respect to its unperturbed location. These longitudinal perturbations are perhaps best visualized

in the resonance frame, which moves into the wave with $v_z = -(\Omega - \omega)/k$ and rotates at Ω; in this frame both the unaffected wave and the unperturbed resonant electron are seen to be stationary in time. In this example, feedback is not included, and hence the phase of $\mathbf{B}_\perp$ is shown to be unperturbed. Thus streams 12 and 6 do not drift, since the corresponding phase angles are always 0 and π, respectively. For $0 < \theta < \pi$ the bunching force is in the $+z$ direction (since q is negative). Thus streams 1–5 will drift backward ($+z$ direction) in the reference frame (which moves in the $-z$ direction at the parallel resonant velocity $v_{\parallel_0}$). For $\pi < \theta < 2\pi$ the drift force is reversed, causing streams 7–11 to drift forward ($-z$ direction). This differential drift causes phase bunching of the 12 helices, as is shown in Figure 3*b* (drawn for a time before the transverse current reaches its first maximum). It must be noted that the situation depicted in Figure 3*b* is located many wavelengths downstream from that of Figure 3*a*, since bunching is a relatively slow process.

As can be seen from Figure 3*b*, a net perpendicular velocity $\sum_{n=1}^{12} \mathbf{v}_{\perp_n}$ has been formed by phase bunching. It is equivalent to a transverse current density $\mathbf{J} = N_E q(1/12) \sum_{n=1}^{12} \mathbf{v}_{\perp_n}$, where N_E is the effective number density of resonant electrons.

Although the representation of Figure 3 is a convenient conceptual model of phase bunching and radiation, it is not well suited to computation because of the continuous nature of the elementary stream. It is desirable to quantize the longitudinal distribution by replacing the continuous helical stream with a series of elementary current sheets. In terms of Figure 3 this quantizing is done by collapsing the cylinder into a flat slab in such a way that the phase of each perpendicular velocity is preserved with respect to the local $\mathbf{B}_\perp$. During this transformation the $\mathbf{v}_\perp$ of each electron follows the helical path of the corresponding elementary stream. The result is an ensemble of 12 elementary sheet currents whose phases are given by the vectors of Figure 3(*a*, *b*). The sheet currents are surface currents whose linear densities $\mathbf{J}_s$ (in amperes per meter) are given by the current density $\mathbf{J}$, multiplied by the length of the cylinder to be represented by the sheet.

An elementary current sheet corresponds to a segment of an elementary stream and is denoted by an initial phase and a position in the stream. In practice, segments of elementary streams as long as 40 wavelengths are represented by a single sheet. The spacing between sheets is chosen so that the change in the wave field between sheets is not more than 10% of the peak amplitude.

The radiation from a current sheet is obtained by regarding the current sheet as a primary source (carefully considering it separately from the cold plasma current, which is induced by the applied wave). From Maxwell's equations we know that a current sheet produces a discontinuity $\mathbf{B}_s$ in $\mathbf{B}_\perp$ whose magnitude (in mks units) is equal to $\mu_0 J_s$, $\mathbf{B}_s$ being perpendicular to $\mathbf{J}_s$. The corresponding electric field $\mathbf{E}_s$, as illustrated in Figure 3*c*, is continuous across the sheet and in antiphase with J_s. This relationship is directly responsible for energy transfer and gives rise in this way to wave growth. It may be helpful to note that these results are precisely analogous to the current and voltage relations on an infinitely long transmission line that is excited by an ideal current generator connected between the conductors. In both cases, waves are launched in both directions perpendicular to the current source. The magnitude of the magnetic field intensity of each of these stimulated waves is $B_s = (\mu_0/2)J_s$.

The signal traveling in the backward ($+z$) direction adds coherently to similar components from the other phase-bunched sheets to form the total stimulated signal. The power for this radiation field is supplied by the deceleration of the gyrating electrons and for each sheet is given by $\mathbf{E} \cdot \mathbf{J}_s$, where $\mathbf{E}$ is the total electric field and $\mathbf{J}_s$ is the sheet current. Summing these products over all sheets gives the total power supplied by the phase-bunched electrons. This value of the power must then equal the net gain in wave power in our model. Although the single sheet shown in Figure 3*c* also excites fields on the right ($-z$ direction), because of their phasing, the end-fire array of sheets produces no significant radiation to the right. Hence $\mathbf{E} \cdot \mathbf{J}_s$ of each sheet contributes only to the whistler-mode wave propagating to the left.

The cold plasma conduction current J_c is a wave-induced current involving only the background electrons and, like the displacement current, is always in quadrature with the wave's electric field. (The displacement current is rela-

tively small and will be neglected here.) This induced current is what accounts for the relatively high value of refractive index (wave number) for the whistler mode but causes only rotation of the total field, not growth. The magnitude of this current is readily obtained by using classical magnetoionic theory. Thus $J_c = N_c q v$, where $v = (q/m)E/(\Omega - \omega)$; for the parameters given below, using $E = v_p B$, where $B = 10^{-12}$ Wb/m², gives $J_c = 3 \times 10^{-9}$ amp/m².

Electron gyrofrequency $\Omega/2\pi$, kHz	33 ($L = 3$)
Plasma frequency $\omega_N/2\pi$, kHz	180 (400 el/cm³)
Wave frequency $\omega/2\pi$, kHz	16.5
Wave phase velocity v_p, km/sec	27,500
Wavelength, meters	1,667
Electron total energy, kev	2.9
Electron parallel velocity $v_\parallel$, km/sec	27,500
Electron pitch angle α, degrees	30
Radius of gyration, meters	77
Interaction length S_i, km	750

The value $J_c = 3 \times 10^{-9}$ amp/m² is to be compared with a typical value of the simultaneous energetic electron source current $J = qN_E\langle v_\perp \rangle \leq 6.1 \times 10^{-12}$ amp/m², where $N_E = 2.4$ m^{-3}. Because the source current is so small relative to the conduction current, it has no significant effect on the propagation of either of the waves, even though it provides the mechanism for wave growth, as is argued above.

Our discussion has implied that the electric field of the wave has no effect on the phase angle θ. At first glance this might seem questionable, since the transverse force $qE_\perp$ exerted by the wave on the electron is of the same order as the longitudinal bunching force $-qv_\perp B_\perp \sin \theta$. However, as was pointed out in *Helliwell* [1970], the phase is affected only by the component of $E_\perp$ that is perpendicular to $v_\perp$. In this case, $E_\perp$ competes with $v_\perp B_0$, which is many orders of magnitude larger (at the equator for $L = 3$, $B_0/B_\perp \approx 10^6$). The resulting perturbation in the effective gyrofrequency is therefore small. The component of $E_\perp$ that is parallel to $v_\perp$ does work on the electron and accounts for the exchange of energy between wave and electrons. This force changes the size and the location of the orbit but does not affect the phase. To test this analysis, $E_\perp$ (including the $\mathbf{v}_\parallel \times \mathbf{B}_\perp$ term) was included in one computer run and was found to have a negligible effect on the currents.

COMPUTER SIMULATION

In this section we set up a computational model for the physical model described in the previous section. For clarity we discuss phase bunching first without feedback and then with feedback.

Cyclotron resonance occurs when the (Doppler shifted) wave frequency seen by the electrons equals their gyrofrequency and is given by

$$\Omega = \omega - k v_{\parallel_0} \tag{1}$$

where $\Omega/2\pi$ is the electron gyrofrequency, $\omega/2\pi$ is the wave frequency, k is the wave number, and $v_{\parallel_0}$ is the parallel velocity of stream (taken positive in the $+z$ direction, i.e., opposite to the direction taken in *Helliwell* [1967, 1970]).

Propagation of the whistler-mode wave is governed by the cold plasma dispersion relation [*Helliwell*, 1965]. When the plasma frequency is much larger than the gyrofrequency, the wave number is given by

$$k = (\omega_N/c)[\omega/(\Omega - \omega)]^{1/2} \tag{2}$$

where $\omega_N/2\pi$ is the plasma frequency and c is the velocity of light.

In the resonance frame the longitudinal force on an electron due to the wave is

$$m\, dv_\parallel/dt = -qv_\perp B_\perp \sin \theta \tag{3}$$

(Note that $v_\parallel = dz/dt$ is now understood to be the departure from the constant resonance velocity $v_{\parallel_0}$.) Longitudinal drift as a result of this force does not change the phase of an electron ($v_y/v_x = $ const, where v_y and v_x are measured in the resonance frame). However, since the wave field is a helix, this drift does change the apparent phase of the local $\mathbf{B}_\perp$ relative to the electron. As is shown in Figure 3*b*, the change in the phase of $B_\perp$ relative to the electron is effectively the same as a phase rotation of each current helix by an amount $d\theta = +k\, dz$, where k is the wave number and dz is the longitudinal displacement measured in the resonance frame. When this relation between angle and displacement is used, (3) becomes

$$d^2\theta/dt^2 + (q/m)kv_\perp B_\perp \sin \theta = 0 \tag{4}$$

which has the same form as the equation for a

simple pendulum. This approximation is commonly employed by other authors[e.g., *Dysthe*, 1971].

The phase perturbation of each of the elementary current sheets is assumed to be governed by (4). When feedback is included, the value of $\mathbf{B}_\perp$ will vary in an unpredictable way from point to point. Hence it is necessary to solve (4) numerically.

Sample computations based on (4) in the absence of feedback are shown in Figure 4*a*. The phase angles between the $\mathbf{v}_\perp$ of each elementary sheet current and the local $\mathbf{B}_\perp$ are shown as a function of time. Summing the currents from the 12 elementary sheets, as determined from Figure 4*a*, gives the total ensemble sheet current density, which is expressed by

$$J_s = \sum_{n=1}^{12} J_n \quad \text{amp/m} \qquad (5)$$

The relative value of this current is normalized to the maximum possible current that would flow if all 12 sheets of the ensemble were exactly in phase and is plotted in Figure 4*b*. It is evident that the actual peak is 70% of the maximum possible value and occurs significantly after the small-angle bunching time (marked by the arrow on Figure 4*a*). Spectral broadening caused by modulation of the parallel velocities is small and will be neglected in the present treatment.

Further examples of the variation of the ensemble sheet current with distance for the nonfeedback case are shown in Figure 5. The solid curve marked $T_w = \infty$ is an extension in distance of the current for CW excitation shown in Figure 4*b*. It clearly shows the anharmonic nature of the total current. The dashed and

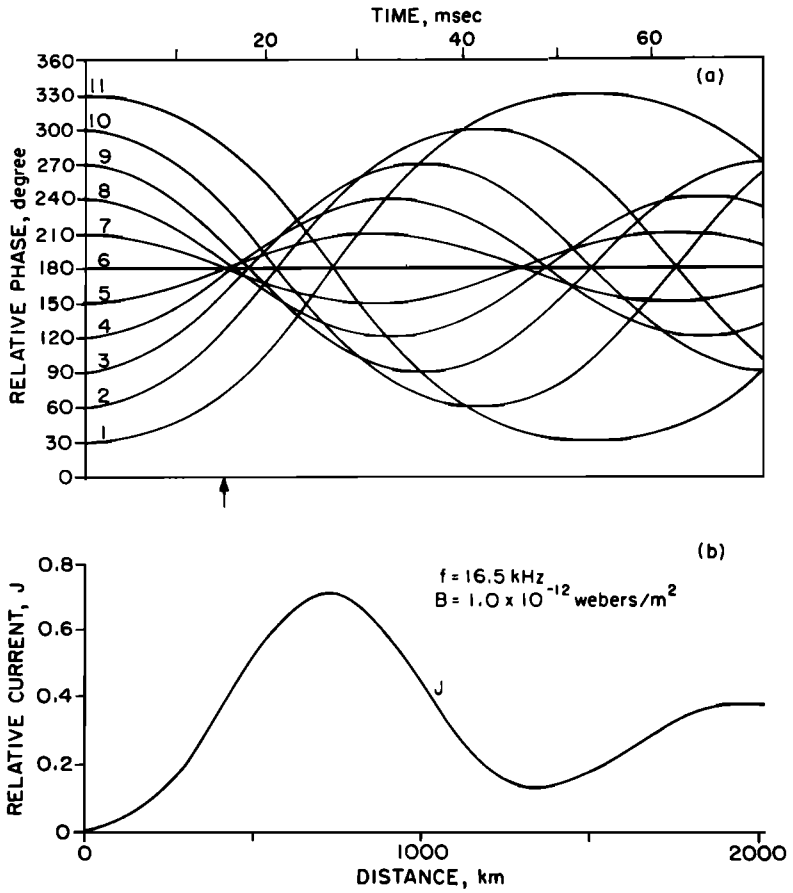

Fig. 4. Elementary sheet currents. (*a*) Variation of phase of the $\mathbf{v}_\perp$ of each elementary current sheet with distance. Small-angle bunching time is marked by arrow. (*b*) Relative magnitude of vector sum of the elementary sheet currents.

broken curves show the sheet current excited by pulses of 100- and 10-msec duration, respectively. Prior to the end of the pulse, the current is identical to the CW case, as is expected. However, after the pulse ends, there is no force to change the longitudinal motion of the elementary sheets, and so their phases continue to change linearly with time. The effect is exactly the same as that for the corresponding set of pendulums when the gravitational force is turned off. The result is that the current eventually reverses. For example, in the case of the 100-msec pulse the ensemble sheet 'sees' the pulse for 50 msec, and the current reverses at about 65 msec.

The relatively long delay of the current peak in the case of the 10-msec pulse illustrates another interesting phenomenon that we shall call 'phase memory.' Here the transverse current is relatively small during the application of the pulse, reaching its maximum value only many pulse lengths later (at 50 msec). During its brief encounter with the sheet ensemble the pulse transfers phase information to each elementary sheet, which in effect receives a different-sized 'kick' depending on its initial phase. After leaving the pulse, each sheet travels at a constant parallel velocity. For the homogeneous model there is no limit to the duration of phase memory. However, in a realistic model, inhomogeneities in the medium and interfering signals would probably prevent the delay from becoming larger than a few tenths of a second. Also, the excitation of off-resonance sheets by a short pulse would cause phase mixing and consequent loss of intensity.

We have just described the production of current through phase bunching of a single 12-sheet ensemble in the absence of feedback. Now we show how to calculate in a self-consistent manner the effect of a sequence of such 12-sheet ensembles on the total field. This is the feedback case. We have seen in Figure 3c how the stimulated current is related to the B_s and E_s of the stimulated wave. The stimulated wave from each ensemble sheet current must be added to the applied wave in the proper way to give the net field at each point in time and space.

To organize the feedback calculations, we use the time-space diagram shown schematically in Figure 6. Five 12-sheet ensembles of equal

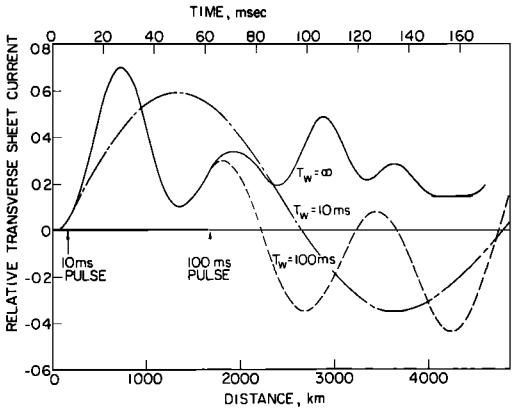

Fig. 5. Relative current versus distance produced by a 12-sheet ensemble excited by constant amplitude pulses of durations of 10, 100, and ∞ msec. Note that the ensemble sheet 'sees' the pulse for one-half the duration of the pulse.

spatial separation are shown entering the wave. Each 12-sheet ensemble is phase-bunched by the total field; at each intersection point on the matrix the stimulated field B_s is calculated by using (5) and is added vectorially to the input field to that matrix point, B_{in}, which includes

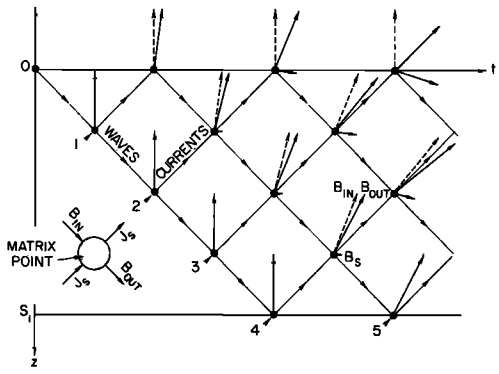

Fig. 6. Schematic space-time matrix showing how stimulated wave fields are added to the total field. The loci of the waves are given by the diagonals slanting downward to the right. The loci of the ensemble current sheets, numbered 1–5, are given by the diagonals slanting upward to the right. The inset diagram shows a typical matrix point, at which the stimulated field B_s is added vectorially to the incoming total field B_{in} to produce the outgoing field B_{out}. This value of B_{out} is applied to the sheet current J_s as it moves to the next matrix point. At each matrix point the magnetic field vector of the incoming wave is shown by a dashed line.

not only the applied field but also all the stimulated components added previously. The total resulting field at a matrix point is labeled B_{out} and is the field applied to the 12-sheet ensemble as it travels to the next matrix point. In this way the total field is continually corrected for the sheet radiation. The sheet current is continuous through each matrix point, as is indicated in the inset diagram of Figure 6. The corrections to the field as seen in the frame of the triggering wave are found by following the diagonal lines slanting downward to the right. The total output field is the value of B_{out} at the upstream edge of the interaction region (bottom horizontal line labeled S_t in Figure 6).

It should be clear from Figure 6 that systematic phase shifts will occur in both the stimulated radiation and the total observed magnetic field. This change in phase results from the 90° phase lag of B_s with respect to J_s (Figure 3c). When the stimulated radiation is relatively large, the phase of the total output signal rotates continuously, amounting to a negative frequency change in the output signal. In the numerical cases to follow, the magnitude of this change is of the order of 10 Hz and is too small to affect significantly the coherence of the stimulated components from different sheets. It should be noted that the separation of matrix points in Figure 6 is exaggerated to illustrate the method of calculation. In the calculations to follow there are 15 sheets occupying an interaction length S_t of 750 km.

RESULTS

An example of CW excitation is shown in Figure 7. Following the plan outlined in the previous section and illustrated in Figure 6, we show the magnitude of the total field as a function of position and time. At the beginning of the output wave form we see the expected increase in field resulting from the stimulated radiation and having a rise time that is close to the bunching time obtained in the absence of feedback. However, as a result of the phase change of the stimulated radiation, the output field pulsates with a period of about 110 msec. This pulsation can be interpreted as beating between the CW input signal and a nearly constant amplitude stimulated signal offset in frequency by −9 Hz.

Similar calculations carried out for different

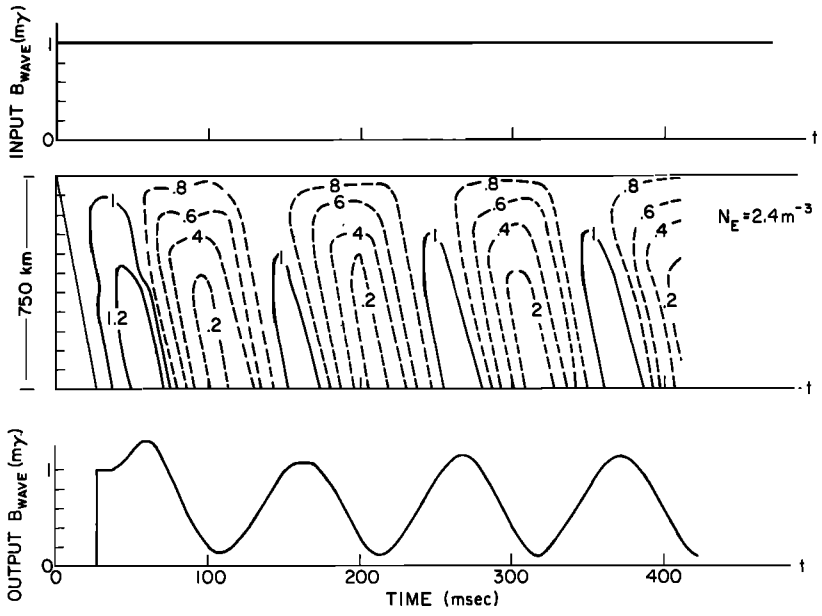

Fig. 7. Example of CW excitation. Middle panel shows space-time matrix of total $B_\perp$ field computed for a continuous triggering signal of 1 mγ and a stream density of 2.4 m^{-3}. Contours show loci of constant total intensity. Solid contours represent total field magnitudes greater than the input field and dashed contours represent reduced magnitudes. The time variations of input and output fields are shown in the upper and lower panels, respectively.

stream densities and different input fields have shown that the average output field can be either greater than or less than the input field. When the stream density is small enough, the stimulated radiation subtracts from the input wave, so that the system become an attenuator. When the amplitude of the stimulated radiation rises above that of the input wave, the average output field increases, and the pulsations decrease in amplitude. Details of this behavior will be reported in a later paper.

To test the validity of our monoenergetic stream model, we have repeated the CW case shown in Figure 7, using a set of streams that is consistent with the energy distribution function measured by *Schield and Frank* [1970]. Up to 11 streams were used, covering a range in pitch angle from 20° to 50° and a range in $v_\parallel$ corresponding to a range of wave frequencies of ±16 Hz with respect to the center frequency. The resonant stream densities varied with pitch angle in accordance with the Schield and Frank energy distribution, an isotropic pitch angle distribution being assumed. The distribution with $v_\parallel$ was assumed flat. The results were qualitatively similar to those for the single pitch angle and the single (resonant) velocity used here.

Much wider ranges of $v_\parallel$ have been employed in this idealized homogeneous model, the results also being very similar to those obtained by using only a single stream. However, Figure 3 of *Helliwell* [1970] shows that the inhomogeneity of the actual magnetosphere results in highly unsymmetric zeroth order (unperturbed) phasing of off-resonant electrons; it is therefore essential that these inhomogeneity effects be included in any realistic assessment of off-resonant electron contributions to the interaction. Because the simulation model results reported here do not include these effects, we have elected not to attempt to refine here the earlier crude estimate of effective bandwidth given in *Helliwell* [1967].

We now turn to the interesting case of excitation by a 10-msec pulse. Curves of the output field versus time are shown in Figure 8*a* for different stream densities. It is seen that the output field reaches its maximum well after the exciting wave is turned off, and thus the phase memory effect shown in Figure 5 is confirmed. For stream densities below a critical value of

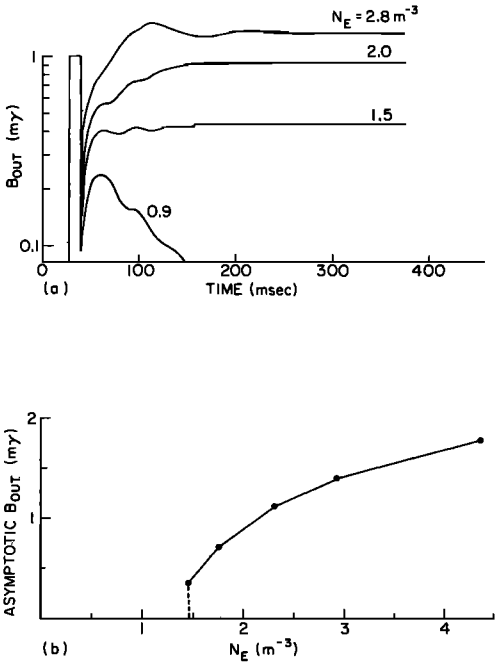

Fig. 8. Response to 10-msec pulse as a function of stream density. (*a*) Output field versus time for 1 mγ, 10-msec exciting pulse, and different stream densities. Oscillations become self-sustaining for stream densities above a 'threshold' of 1.5 m^{-3}. (*b*) Variation of asymptotic value of output estimated from Figure 8*a* versus stream density. At the threshold value of N_E the steady state output jumps to the minimum value of 0.3 mγ.

1.5 m^{-3} the output first rises to a peak and then decays to zero. Above this critical stream density the oscillation is self-sustaining, and the output approaches a steady limiting value.

The variation of the limiting amplitude of Figure 8*a* versus stream density is shown in Figure 8*b*. There is a sudden jump at N_E = 1.5 m^{-3}, where self-sustaining oscillations begin. The curve then begins to level off, suggesting that there may be a maximum output regardless of the density of the stream. Results for higher stream densities are not shown because then our assumption of slowly varying conditions breaks down.

After the oscillation amplitude becomes constant, as is shown in Figure 8*a* for $t > 200$ msec, a steady state is reached at all locations within the emission cell. We can then examine the field and current relations as a function of distance

only. To illustrate, we use the case shown in Figure 8*a* with $N_E = 2.8$ m^{-3}. Since we are now dealing with the steady state, it is appropriate to use a continuous spatial distribution based on the discrete sheets of the model. Thus the current density J in amperes per square meter is the linear sheet current density divided by the spacing between the sheets. The total field $B_\perp$, the current density J in amperes per square meter, and the phase angle between $\mathbf{E}_\perp$ and $\mathbf{J}$ are plotted in Figure 9*a*. As is expected, the stimulated current begins with zero slope at the output of the cell, following a curve similar to that for the nonfeedback case shown in Figure 4*b*. The reason these current curves are similar is that most of the momentum for phase bunching is imparted to the electrons in the left-hand part of the cell, where $B_\perp \approx$ const. Accordingly, we call this region the 'buncher.'

As electrons enter the buncher, the initial current is parallel to $B_\perp$ and hence perpendicular to $\mathbf{E}_\perp$ (as is clear from Figures 2 and 3). Thus no power is abstracted initially from the resonant electrons. However, as the sheet ensemble moves through the cell, it sees a slow rotation of $\mathbf{B}_\perp$ as a result of the previous generation of $\mathbf{B}_s$ components that lag the current by 90°. This rotation accounts for the nonzero slope of ϕ_{JE} at the entrance to the cell.

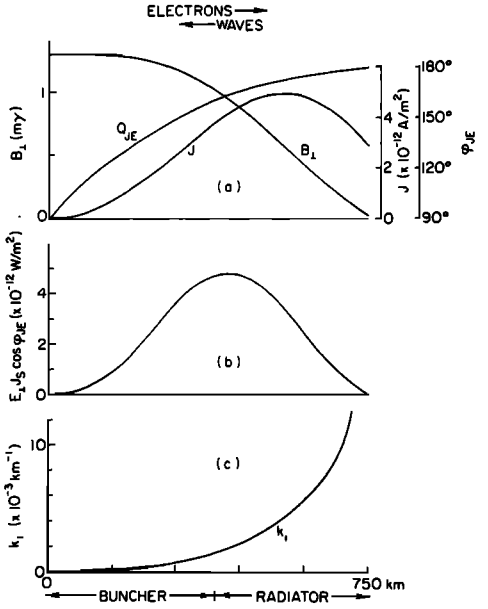

Fig. 9. Interaction region cross section during self-sustained emission. (*a*) Steady state spatial variations of $B_\perp$, J_s, and ϕ_{JE} for self-excited oscillations, where $N_E = 2.8$ m^{-3}. (*b*) Power density generated by phase-bunched electrons. (*c*) Growth rate k_i computed from Figure 9*a*.

On the right-hand side of the cell there is no input wave, so that the entire wave field is created by the local $\mathbf{J}$, giving $\phi_{JE} = 180°$. Power transfer is then a maximum. Accordingly, we shall call the right-hand side of the cell the 'radiator.' The phase angle ϕ_{JE} varies smoothly from 90° to 180° (Figure 9*a*).

Power production is shown in Figure 9*b* and is given by $E_\perp J \cos \phi_{JE}$. Accordingly, it must be zero at the left (where $\phi_{JE} = 90°$) and zero at the right (where $E_\perp = 0$). Maximum power is produced slightly to the right of the center of the cell, where $E_\perp$ and $J_\perp$ are near their maximum values and ϕ_{JE} is close to 180°. The spatial growth rate of the field components, shown in Figure 9*c*, has a different shape, since the power required for a given growth rate depends on the amplitude of the signal. The growth rate approaches infinity on the right, since the system is a self-excited oscillator, and hence there is no input field to be amplified.

The effect of changing the amplitude of a 10-msec exciting pulse by factors of 10 while N_E is held constant is shown in Figure 10*a*. It is evident that the final output of the self-sustained oscillation is independent of the applied field, as is expected. However, both the time required to reach maximum and the shape of the rising portion of the curve depend upon the pulse amplitude. For sufficiently weak applied signals the initial growth of the self-sustained oscillation is clearly exponential, the temporal growth rate being $\gamma = 23$/sec. For the more intense triggering signals (0.1 and 1 mγ) the same exponential growth applies over a portion of each curve. Each reduction of the applied field by a factor of 10 increases the delay of the self-sustained oscillation by 100 msec. We conclude that for this one-dimensional model with $N_E = 2.8$ m^{-3} the oscillation will be self-sustaining regardless of how small the triggering signal may be. The exponential growth rate varies linearly with stream density (Figure 10*b*).

Figure 8 shows that, when N_E exceeds the critical density, an impulse can trigger a self-sustaining emission; Figure 10*b* shows that, when self-sustaining emissions are possible, any

impulse, no matter how small, will initiate the growth process. Since weak noise is always present in the magnetosphere, we must explain why emissions are not observed except when suitable triggering signals are present.

A possible answer lies in the limitations of our one-dimensional model. In the actual magnetosphere we expect that there must be a limit to the lateral extent of coherent wave-particle interaction. The emission cell can be pictured as a sausage-shaped region several hundred wavelengths long and at least a few wavelengths wide. Many such cells could exist in a single whistler duct that may have a diameter of several hundred kilometers [*Angerami*, 1970]. The finite width of the emission cell will introduce a geometrical spreading loss in the radiation, causing a reduction in the fields available to bunch new electrons. There is also no allowance in the model for interference from other waves or for scattering of the waves by transverse inhomogeneities of the medium. All of these effects would reduce the intensity of the waves appearing in the bunching region for a given stream density. Their effect therefore is roughly equivalent to reducing the stream density in our model. Thus some excess of electrons over the calculated threshold value is required to compensate for these propagation losses.

We can now see the outline of a more realistic model in which the initial waves of a spontaneous emission, assumed to originate in a small volume of space, will diverge as they travel toward the bunching region. This divergence represents a net loss of gain in the feedback loop and amounts to lowering the stream density below the threshold level, making growth impossible. The smaller the initial wave loss, the greater the probability that a self-sustaining oscillation will develop.

Similarly, a self-sustaining emission would terminate when the bunching wave intensity is sufficiently reduced. Increased attenuation between the radiator and the buncher could result from changes in the location of the interaction region or in the frequency of the oscillation.

Using the idea of a spreading-loss-dependent effective stream density, we can understand why external triggering signals may stimulate emissions at times when there are no spontaneous emissions. We assume that the injected

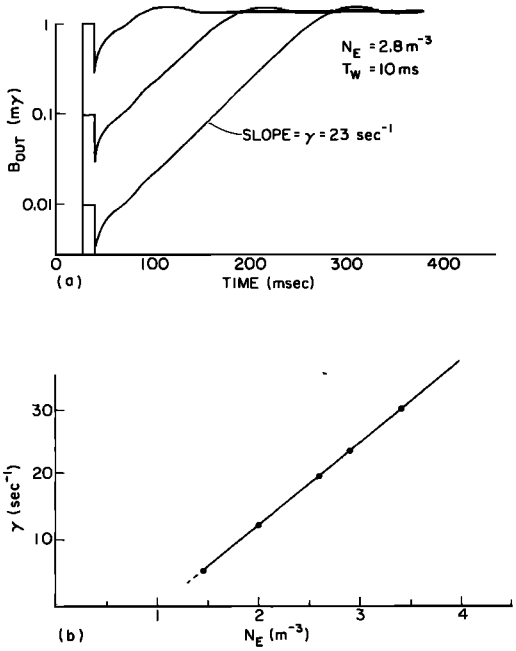

Fig. 10. Response to 10-msec pulse as a function of pulse amplitude. (*a*) Logarithm of the output field versus time for 10-msec pulse of variable amplitude (1, 0.1, and 0.01 mγ) and a stream density of 2.8 m^{-3}. An exponential growth rate of $\gamma = 23$ sec^{-1} is indicated by the straight-line segments of the curves. (*b*) Variation of the exponential growth rate shown in Figure 10*a* with stream density. Growth rate is zero below the threshold density of 1.5 m^{-3}.

wave originates at a distant point and therefore illuminates an area much larger than the cross section of an emission cell. Initial bunching then occurs over the full width of the emission cell, causing the initial divergence loss to be reduced. The effective stream density then exceeds the threshold value, causing self-sustaining oscillations to develop. The same argument explains why triggered emissions usually contain more components than isolated spontaneous emissions: the triggering wave is able to fire many emission cells at nearly the same time, causing an increase in total emission power and bandwidth compared with spontaneous emissions.

Preference for triggering at one-half the gyrofrequency is explained in the same way. Divergence of energy from a finite source is reduced because of the increased flatness of the refractive index surface at this frequency. (It is essentially flat at this frequency for wave normal directions

within 20° of $\mathbf{B}_0$.) Thus most of the wave energy is collimated along $\mathbf{B}_0$, giving maximum intensity in the bunching region for a given stream density.

COMPARISON WITH OBSERVATIONS

Evidence confirming the predicted amplitude pulsations of Figure 7 is found in two recent reports on pulsations of whistler-mode echoes. The first describes pulsations in a key-down transmission from station NAA [*Bell and Helliwell*, 1971]. There are two pulsation periods, the longer one (580 msec) occurring at the measured one-hop whistler travel time over the path. Between these pulsations are regular deep pulsations of lower peak amplitude. Their period is 140 msec, roughly one fourth of the longer period. It is this shorter-period pulsation that we wish to compare with our theory. A portion of the published record is replotted in Figure 11*b*.

The second example of pulsations is found in the observation of an 800-msec whistler-mode pulse excited by a Russian transmitter on 15 kHz [*Likhter et al.*, 1971]. The envelope of their published oscillogram, replotted in Figure 11*c*, shows a period of 180 msec, as compared with 140 msec for the NAA pulsations. For comparison with these experimental observations the prediction of our model (110 msec), as shown in Figure 7, is replotted in Figure 11*a*. Since the pulsation period depends on various parameters of the model that may vary with conditions, this degree of agreement in period is considered satisfactory. Perhaps more important is the fact that both experiments show deep fading, indicating that the stimulated component is comparable in magnitude to the triggering waves.

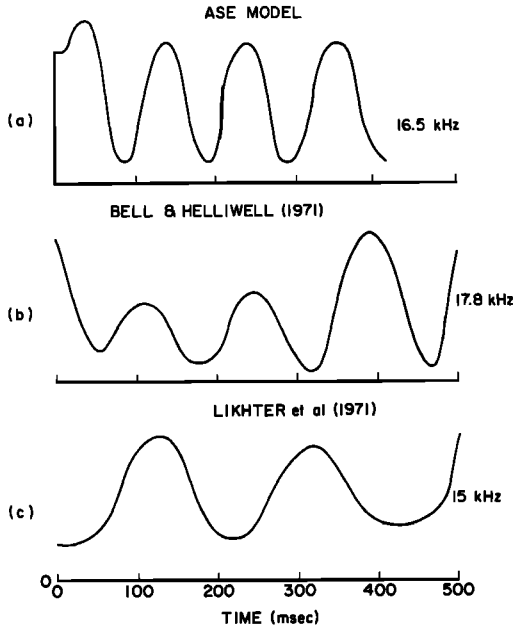

Fig. 11. Comparison of model results with published data. (*a*) Initial part of theoretical pulsation replotted from Figure 7. (*b*) Portion of observed natural pulsations from NAA on 17.8 kHz [*Bell and Helliwell*, 1971]. (*c*) Replot of envelope of pulsating whistler-mode signal observed from Russian transmitter on 15 kHz [*Likhter et al.*, 1971].

The delay in the onset of self-sustaining oscillations predicted by Figure 10 has also been seen in some experimental data. An example of this effect is illustrated by Figure 12, which shows nose whistlers that trigger narrow-band emissions near the upper cutoff of the whistlers. The emissions are seen to be self-sustaining and nearly monochromatic, in agreement with the model results in Figures 8 and 10. Several of these emissions also show quite clear separations from the trace of the triggering whistler. The magnitude of this separation is about 100 msec and can be explained in terms of the delay shown in Figure 10.

Another test of the predictions of our model can be found in the amplitude behavior of whistler echo trains. It is often observed that echo trains continue for extended lengths of time but do not show appreciable growth. In one unusual example several hundred echoes were observed, there being very small attenuation between successive echoes [*Helliwell*, 1965]. An explanation given by *Liemohn* [1967] assumed that the growth rate is independent of intensity and that the integrated growth and loss rates were equal over the path. This assumption implies the occasional occurrence of echo trains in which the intensity increases systematically with the order of the echo; none has been reported. We suggest instead that these nearly constant amplitude echo trains result from the saturation effect predicted by our model. Thus, if the input signal level is high, the gain is low. On the other hand, if the level is low, the gain is high. We conclude there-

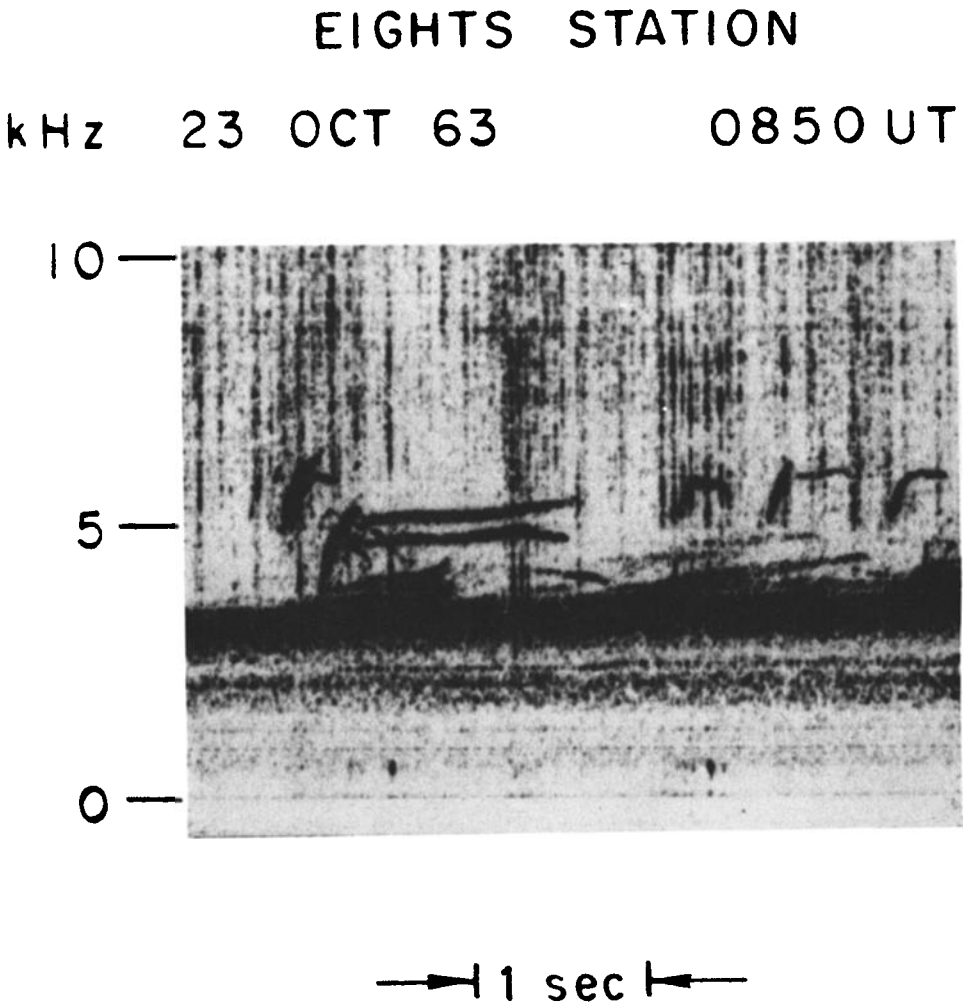

Fig. 12. Spectrogram of narrow-band emissions triggered by whistlers near their upper-cutoff frequency. Onset of some emissions is delayed by an estimated 100 msec.

fore that the gain adjusts itself automatically so as to equal exactly the total path loss.

Certain features of ASE can now be understood in terms of our model. We suppose that a strong signal will interfere with the establishment of a feedback loop at a nearby frequency by disorganizing the phases of the electrons that are resonant at the new frequency. However, where the total signal is weak, a weak stimulated wave component at a nearby frequency could grow and might reach sufficient amplitude to be immune to further debunching by the triggering wave. Such a situation is in fact suggested by Figure 7, which shows a periodic trough in total field intensity extending over about half the interaction region. Electrons traversing this trough would be free to respond to the bunching action of new frequency components generated by the inhomogeneities of the medium. Thus the new oscillation might be expected to emerge from the background noise with a delay of about 100 msec, just as is observed.

For triggering pulses of less than about 50 msec in duration the trough pattern of Figure 7 would not have time to develop before termination of the triggering wave. Thus the growth of a new emission at an offset frequency could be prevented, thereby accounting for the rela-

tively infrequent triggering of emissions by Morse dots, as compared with Morse dashes.

In the case of positive frequency offsets, the frequency of the new oscillation is not easy to determine, since both off-resonance electrons and the change in Ω can produce new frequencies. In view of the fact that virtually all initial frequency offsets are positive (G. S. Stiles, private communication) we suppose that the spatial inhomogeneity is the controlling factor, as was previously suggested [*Helliwell*, 1967]. For example, consider a round trip delay of 50 msec, the electrons traveling for 25 msec at a velocity of 2.75×10^7 m/sec after leaving the center of the emission cell on the equator. The corresponding distance is 690 km. From *Helliwell* [1967], using $\Delta\Omega = \Omega_0[4.5 \times (690/19{,}100)^2]$ and (1) and (2) and neglecting the change in $v_\parallel$ due to the nonzero pitch angle, we find the corresponding wave frequency change to be 145 Hz. We assume that this frequency shift is produced by a sheet that crosses the center of the emission cell when the field there is a maximum (~40 msec on Figure 7). It then takes 50 msec for the offset stimulated radiation at 145 Hz to return to the equatorial region, where it grows to produce the offset 'plateau' seen on many ASE. We estimate that about 30–40 msec is required for the new oscillation to reach the threshold of detection, giving the observed total delay of about 100 msec with respect to the leading edge (~30 msec on Figure 7) of the triggering signal. The plateau is thought to exist because the triggering signal continues to generate a train of offset waves of constant spectrum. When the carrier amplitude falls, owing to fading (Figure 7) or signal termination, the emission cell is free to drift downstream, where rising tones are produced.

EXTENSION OF MODEL

An important extension of our model will be the inclusion of the inhomogeneity of the medium. Referring to Figure 6, we might view each matrix point as having a unique set of parameters for both the wave and the medium. Furthermore, generated waves plus input waves at each matrix point would diverge in traveling to the next matrix point in accordance with the assumed properties of the emission cell. Provision should also be made for including two or more triggering frequencies at one time.

One of the main reasons for extending the model in this way is to explain the generation of new frequencies. One source of frequency change is the inhomogeneity of the medium. Its role in controlling df/dt has already been discussed in *Helliwell* [1967, 1970]. Other sources of new frequencies are the not quite resonant electrons that are partially bunched by the waves.

The effect of changing frequency on the results reported here remains to be explored. However, the analysis given in *Helliwell* [1970] shows that the phasing between electrons and waves is independent of df/dt to first order. Thus we would expect to observe about the same amplitude variations on gliding tones that are seen on constant frequency signals.

CONCLUSIONS

In summary, we find that the feedback model developed in this paper predicts a number of observed phenomena including (1) pulsations, (2) delay in onset of self-sustained oscillations, and (3) variable gain. The general nature of these results and the fact that they are not found by using other theories suggest the importance of feedback and the initial value approach to the problem.

The theory may have several useful applications. Possible areas of interest include diagnostics of energetic particles, communications, plasma physics, and modification of the upper atmosphere. With the computer model employed here it is a relatively straightforward task to compute the pitch angle scattering for representative test electrons. By means of this result the flux of precipitated particles can be computed. This model will aid in developing new experiments using man-made triggering signals.

It may be useful to note some similarities between the wave-electron interaction discussed here and other wave-particle interactions. *Brice* [1964*b*] has pointed out that the interaction of energetic protons with hydromagnetic waves (~1 Hz) is analogous to the interaction of energetic electrons and VLF whistler-mode waves. *Smith* [1972] notes in his review of pulsars that cyclotron interaction between the pulsar waves and the relativistic electrons is a

promising mechanism, but no coherence mechanism has yet been developed. The present theory may have applications to these two topics.

Finally, we call attention to the more general problems of wave-particle interaction in laboratory plasmas, where coherent wave generation through feedback may play a role.

Acknowledgments. The authors thank A. L. Brinca for helpful discussions and T. F. Bell for his suggestions and critical reading of the manuscript.

The work was sponsored by the Air Force Office of Scientific Research under grant F4462-72-C-0058.

* * *

The Editor thanks R. L. Dowden and R. Gendrin for their assistance in evaluating this paper.

REFERENCES

Angerami, J. J., Whistler duct properties deduced from VLF observations made with the Ogo 3 satellite near the magnetic equator, *J. Geophys. Res., 75,* 6115, 1970.

Bell, T. F., and R. A. Helliwell, Pulsation phenomena observed in long-duration VLF whistler-mode signals, *J. Geophys. Res., 76,* 8414, 1971.

Brice, N., An explanation of triggered VLF emissions, *J. Geophys. Res., 68,* 4626, 1963.

Brice, N., Fundamentals of VLF emission generation mechanism, *J. Geophys. Res., 69,* 4515, 1964*a*.

Brice, N., Discrete VLF emissions from the upper atmosphere, Ph.D. thesis, Dep. of Elec. Eng., Stanford Univ., Stanford, Calif., Aug. 1964*b*.

Burtis, W. J., and R. A. Helliwell, Banded chorus—A new type of VLF radiation observed in the magnetosphere by Ogo 1 and Ogo 3, *J. Geophys. Res., 74,* 3002, 1969.

Carpenter, D. L., Ducted whistler-mode propagation in the magnetosphere; A half-gyrofrequency upper intensity cutoff and some associated wave growth phenomena, *J. Geophys. Res., 73,* 2919, 1968.

Dysthe, K. B., Some studies of triggered whistler emissions, *J. Geophys. Res., 76,* 6915, 1971.

Gendrin, R., Gyroresonant wave-particle interactions, in *Solar-Terrestrial Physics/1970,* edited by E. R. Dyer, pp. 236–269, D. Reidel, Dordrecht, Netherlands, 1972.

Helliwell, R. A., *Whistlers and Related Ionospheric Phenomena,* Stanford University Press, Stanford, Calif., 1965.

Helliwell, R. A., A theory of discrete VLF emissions from the magnetosphere, *J. Geophys. Res., 72,* 4773, 1967.

Helliwell, R. A., Low-frequency waves in the magnetosphere, *Rev. Geophys. Space Phys., 7,* 281, 1969.

Helliwell, R. A., Intensity of discrete VLF emissions, in *Particles and Fields in the Magnetosphere,* edited by B. M. McCormac, pp. 292–301, D. Reidel, Dordrecht, Netherlands, 1970.

Kimura, I., On observations and theories of the VLF emissions, *Planet. Space Sci., 15,* 1427, 1967.

Liemohn, H. B., Cyclotron-resonance amplification of VLF and ULF whistlers, *J. Geophys. Res., 72,* 39, 1967.

Likhter, Ya. I., O. A. Molchanov, and V. M. Chmyrev, Modulation of spectrum and amplitudes of low-frequency signal in the magnetosphere plasma, *Sov. Phys. JETP Lett., 14,* 325, 1971.

Schield, M. A., and L. A. Frank, Electron observations between the inner edge of the plasma sheet and the plasmasphere, *J. Geophys. Res., 75,* 5401, 1970.

Smith, F. G., Pulsars, *Rep. Progr. Phys., 35,* 399, 1972.

(Received April 4, 1973;
accepted July 31, 1973.)